Applied Clay Science 139 (2017) 20–27

Contents lists available at ScienceDirect

Applied Clay Science

journal homepage: www.elsevier.com/locate/clay

Research paper

Effects of montmorillonite (Mt) and two different organo-Mt additives on the performance of asphalt

M.A. Vargas [a,*], L. Moreno [b], R. Montiel [c], O. Manero [b], H. Vázquez [c]

[a] Tecnológico de Estudios Superiores de Ecatepec, TESE, Av. Tecnológico S/N C.P. 55210 Col. Valle de Anáhuac, Ecatepec de Morelos, Estado de México, México
[b] Instituto de Investigaciones en Materiales, Universidad Nacional Autónoma de México, A.P. 70-360, México D.F. 04510, México
[c] Universidad Autónoma Metropolitana-Iztapalapa, Depto. Física, Av. San Rafael Atlixco No. 186, Col. Vicentina, Iztapalapa 09340, México

ARTICLE INFO

Article history:
Received 23 August 2016
Received in revised form 6 January 2017
Accepted 7 January 2017
Available online 20 January 2017

Keywords:
Asphalt
Nanocomposites
Morphology
Viscoelastic
Rutting
Zero shear viscosity

ABSTRACT

In this work, comparative rheological tests on asphalt mixtures containing unmodified Montmorillonite (Mt) and two modified organo-Mt were carried out. The blended asphalt binders were characterized using softening point, penetration, and rheological tests, and compared with the unmodified asphalt. The nanostructure distribution of Mt platelets in asphalt was evaluated using X-ray diffraction (XRD), TEM and fluorescence microscopy. An increase in the softening point and a decrease in binder penetration were observed upon the addition of nanoparticles. Also, the elastic modulus (G′) increased significantly at low frequencies and high concentration of nano-Mt. Asphalt and nanocomposites are thermo-rheologically simple materials; the temperature dependence was modeled using the time-temperature superposition principle. The complex viscosity of 10 wt.% trimethyloctadecacylammonium chloride (TMOA) in asphalt increased in two decades, whereas that of the aminopropyl-triethoxysilane/octadecyl-amine (APTES) and Mt at the same concentration increased only in one decade. The G*/sinδ values and viscosity analyses revealed that the TMOA-modified asphalt exhibited an improved viscoelastic response and resistance to rutting. Organo-nanocomposite modified-asphalt generates an intercalated structure, as revealed by X-ray diffraction (XRD) and transmission electron microscopy (TEM). Zero shear viscosity (ZSV) is important to predict the rutting behavior of asphalt binders. The ZSV of asphalt and nanocomposites were calculated using the Cross and the Carreau models.

1. Introduction

Nowadays, nanotechnology has gradually been incorporated into the field of modified asphalt (You et al., 2011; Fang et al., 2013; Yang and Tighe, 2013; Golestani et al., 2015). Nano-modified asphalt offers a significant improvement of the key material properties, and often is superior to other asphalt modification methods. Certain inorganic metal oxide nanomaterials have achieved a dominant position as asphalt binders, among which the most widely used has been the layered clay minerals, primarily Mt (Montmorillonite), which has a 2:1 layered structure with two silica tetrahedral sheets sandwiching an alumina octahedral sheet. Mt is usually modified using quaternary ammonium salts with alkyl chains, rendering the layered silicate organophilic, with enlarged interlayer space (Yu et al., 2007; Jahromi and Khodaii, 2009; El-Shafie et al., 2012). Upon adding the nanoclay minerals to the asphalt and/or polymeric matrix, and mixing them at high temperature, its molecules can penetrate between the silicate layers. Different structural morphologies can be observed, which depend on the degree of the dispersion of the clay minerals platelets: agglomerated, intercalated structure, and exfoliated structure (Zare-Shahabadi et al., 2010; Santagata et al., 2015). The effects of sodium montmorillonite (Mt) and organo-montmorillonite (OMt) on the physical properties of asphalt have been investigated elsewhere (Polacco et al., 2008; Merusi et al., 2012; Liu et al., 2013; Chen et al., 2015; Ortega et al., 2015). Results show that Mt improved the physical properties, rheological behavior and the storage stability of asphalts, and the organo-Mt exhibited better modifying effects on the asphalt (Liu et al., 2010; Zhang et al., 2011; Yao et al., 2012; Yao et al., 2013). In addition, the structure of asphaltenes in asphalt depends on the chemical composition of the binder and on temperature. Thus asphalts with lower asphaltenes proportion have weak Mt-asphalt interactions which limit their ability as binders in asphalt-nanoparticles systems (Jahromi et al., 2010). In combination with Mt, coupling agents such as silane, are used for Mt surface modification and to disperse it. In fact, silane coupling agents enhance the affinity of organo-Mt to the polymer matrix (Yu et al., 2009; Sureshkumar et al., 2010; Golestani et al., 2012; Min et al., 2015).

The interest on rheological properties of asphalt/nanocomposites is based on the analysis of the transition from the conventional liquid-like behavior to the so-called pseudo-solid-like response upon increasing nanofiller content and the presence of a modifier polymer (Drozdov et al., 2008).

* Corresponding author.
E-mail address: angelesvhg@gmail.com (M.A. Vargas).

http://dx.doi.org/10.1016/j.clay.2017.01.009
0169-1317/

The main objectives of this research are as follows:

1) Analysis of the effect of different types of nanoparticles (Mt, TMOA and APTES) on the physical and rheological properties of asphalt, for which fluorescence microscopy, X-ray diffraction, TEM, and rheological tests were applied;
2) Comparison of the different models and methods available to calculate the ZSV of asphalt nanobinders.

2. Background

The response of conventional asphalts under small shear stresses is linear and their viscosity is independent of shear rate. In contrast, polymer-modified asphalts (PMAs) are pseudo-plastic fluids with a rheological response that depends on the shear rate. However, for very low shear rates, this behavior turns less complex and becomes similar to conventional asphalts. In this case, the energy is dissipated until the viscosity of asphalt reaches a constant value independent of shear rate. This viscosity is called Zero Shear Viscosity (ZSV) and is a material property of the asphalt. The ZSV is an indicator of two rutting related binder characteristics, namely, the stiffness and binder resistance to permanent deformation under long term loading (Biro et al., 2009).

Asphalt behavior is generally characterized by decreasing viscosity with increasing frequency between two well-defined values: Zero Shear Viscosity (η_0) at zero frequency and limiting viscosity (η_∞) at an infinitely high frequency (Morea et al., 2010). For low frequencies, viscosity data tend to a plateau; a trend that is clearly visible in conventional asphalts. However, for some asphalts there is no such plateau.

2.1. Prediction of ZSV based on Carreau's model

The Carreau's model is used to determine the ZSV for the all blends, Eq. (1). The ZSVs of the different systems are shown in Fig. 6 according to:

$$\eta^* = \frac{\eta_0 - \eta_\infty}{\left[1 + (K\omega)^2\right]^{m/2}} + \eta_\infty \quad (1)$$

η^* is the complex viscosity, η_0 is the first Newtonian viscosity, η_∞ is the infinite shear viscosity, ω is the frequency (rad/s), K and *m* are material parameters.

2.2. ZSV determination based on Cross/Williamson's model

Data from a frequency sweep test was described by the Cross/Williamson's model, Eq. (2). The data was then extrapolated to zero frequency in order to determine the ZSV of the binders (Fig. 6).

$$\eta^* = \frac{\eta_0 - \eta_\infty}{1 + (K\omega)^m} + \eta_\infty \quad (2)$$

where η^*, η_0, η_∞, ω, K, and *m* are defined as in Eq. (1).

2.3. ZSV determination based on the Cross/Sybilski's model

Similarly, the data from the frequency sweep tests were described by the Cross/Sybilski's model using Eq. (3). The ZSVs calculated by extrapolating the data to a zero frequency are shown in Fig. 6.

$$\eta^* = \frac{\eta_0}{1 + (K\omega)^m} \quad (3)$$

3. Experimental

3.1. Materials

Asphalt AC-20 from PEMEX, México, has the following physical properties: penetration: 67 dmm (25 °C, ASTM standard D5); softening point: 49 °C (ASTM standard D36) and the solubility test in n-heptane (ASTM standard D2042) gives 80 wt.% maltenes and 20 wt.% asphaltenes.

Sodium Mt from Nanocor Inc. (Arlington Heights, IL, USA) with ionic interchange capacity of 135 meq/100 g, specific gravity of 2.6, and mean particle size of 22 μm, was used as the dispersed phase. Two organo-Mt were used in asphalt AC-20; 1) trimethyloctadecacyl ammonium chloride (TMOA) containing 25–30 wt.% trimethyl stearyl ammonium, and 2) nanoclay, surface-modified, which contains 0.5–5 wt.% amino propyl-triethoxysilane (APTES), 15–35 wt.% octadecyl-amine matrix. They were used as received from Sigma-Aldrich Chemie GmbH (México City, México).

3.2. Preparation of Mt and OMt modified asphalt

The modified asphalt was prepared using a high-shear mixer. Asphalt was heated up to melting at around 150 °C in an iron container. Then three percentages (2%, 5% and 10% by weight) of the various nanoparticles (Mt, TMOA and APTES) were added to the base asphalt with continuous stirring (2500 rpm) at 160 °C for two hours. High homogeneity was reached, producing various blends: A/Mt2, A/Mt5, A/Mt10, A/TMOA2, A/TMOA5, A/TMOA10, A/APTES2, A/APTES5 and A/APTES10. All the prepared binders were left to cool at room temperature. Asphalt AC-20 was also processed under the same conditions for comparison with the modified asphalt.

3.3. Physical properties test

Softening point and penetration (25 °C) were tested according to ASTM D36 and ASTM D5, respectively.

3.4. Fluorescence microscopy

Fluorescence microscopy tests were performed with a Carl-Zeiss KS 300 microscope at ambient temperature with a wavelength of 390–450 nm with an objective power of 20× and eyepiece lens of 10×. Micrographs were taken with a MC100 camera equipped with an automatic counter. In the nanocomposite A/TMOA, the particle size distribution and shape were measured as the quaternary ammonium surfactant shows fluorescence (Kakehi et al., 1997). Mt and APTES did not present fluorescence.

3.5. X-ray diffraction (XRD)

X-ray diffraction tests were measured in air at room temperature using a Bruker D-8 Advance diffractometer with the θ-2θ geometry, Cu Kα radiation, a Ni 0.5% Cu-Kβ filter in the secondary beam, and a one-dimensional positive-sensitive silicon strip detector (Bruker, Lynxeye). The diffraction intensity as a function of 2θ angle was measured between 0.5 and 10.0°, with a 2θ step of 0.02037°, for 0.400 s per point.

3.6. Transmission electron microscopy (TEM)

A morphological investigation of the dispersion in the materials was carried out by means of a high-resolution transmission electron microscope (HRTEM JEOL 2100F) with acceleration voltage of 200 kV.

3.7. Rheological measurements

Dynamic measurements were performed in parallel-plate fixture, under stress-controlled mode AR-G2 (TA Co., USA). A frequency sweep from 0.1 to 100 rad/s at different temperatures (25, 40, 60, 75 and 100 °C) was applied at a fixed strain in the linear viscoelastic region. Smooth plate-and-plate geometry with 25 mm diameter and 1 mm gap was used for the whole set of samples. A stabilization time of 15 min was allowed for each sample.

Table 1
Effects of Mt and organo-Mt on softening point and penetration of asphalt. Apparent activation energies for pure asphalt and nanocomposites.

		Mt content (wt.%)			TMOA content (wt.%)			APTES content (wt.%)		
Physical properties	Asphalt	2	5	10	2	5	10	2	5	10
Softening point (°C)	49	50	53	57	53	56	60	51	54	58
Penetration (dmm)	67	64	61	58	62	58	53	65	62	60
E_a(kJ/mol)	58	64	67	70	61	66	68	62	62	61

4. Results and analysis

4.1. Physical properties

The softening point of the Mt-modified asphalts gradually increases as a function of Mt or organo-Mt content (Table 1). This effect is associated with the presence of nanoparticles forming intercalated/exfoliated structures in the asphalt matrix. TMOA-modified asphalts exhibit a remarkable improvement in the softening point in comparison to the other samples. TMOA-nanoclay can form intercalated structures in the asphalt matrix due to its organophilic character, which confers more compatibility with the asphalt (maltenes). As a result, the A/TMOA systems are more stable to high temperatures and may also be more resistant to permanent deformation (rutting) compared to the unmodified asphalt, according to the results shown in Table 1 (El-Shafie et al., 2012). A/APTES brings little change in penetration and softening point with respect to the unmodified asphalt. This slight enhancement observed for A/APTES is lower than that of A/TMOA, but similar to that of A/Mt.

4.2. Fluorescence microscopy

The morphology and dispersion of the TMOA nanoparticles in asphalt are shown in Fig. 1. Scarce fluorescent material is present in the base asphalt, so that the micrographs are generally dark, as shown in Fig. 1a. In contrast, it is easier to observe TMOA particles under the same conditions due to their fluorescence. A/TMOA2, A/TMOA5 and A/TMOA10 are shown in Fig. 1b–d, respectively. A/TMOA2 binder shows poor phase dispersion of small dots distributed throughout the asphalt (Fig. 1b) where the bright TMOA phase and dark asphalt phase are easily distinguished. As TMOA content increases, the boundary between bright and dark areas becomes sharper (A/TMOA5 in Fig. 1c), whereas fine white nanoparticles are evenly dispersed in the A/TMOA10 blend (Fig. 1d). In this case, compatibility of A/TMOA is relatively high, which could explain the viscosity behavior, softening point, and penetration. This, in turn, may be caused by a higher interaction of non-polar organo-Mt with the non-polar component of asphalt (maltenes).

4.3. XRD analysis

The dispersion of the silica layers in the asphalt matrix was determined by the interlayer space. The *d*-value is calculated by means of the 2θ angle value at which basal reflection is observed (Bragg equation):

$$n\lambda = 2d\ \sin\theta \tag{4}$$

λ is the X-ray wavelength (for Cu, λ = 0.15418 nm), *d* is the interlayer distance, n is the order of diffraction, corresponding to an integer multiple of the wavelength, and θ is the angle of incident radiation. The XRD results for pure Mt and A/Mt composites are shown in Fig. 2a at different concentrations. Since Mt and their nanocomposites do not show any

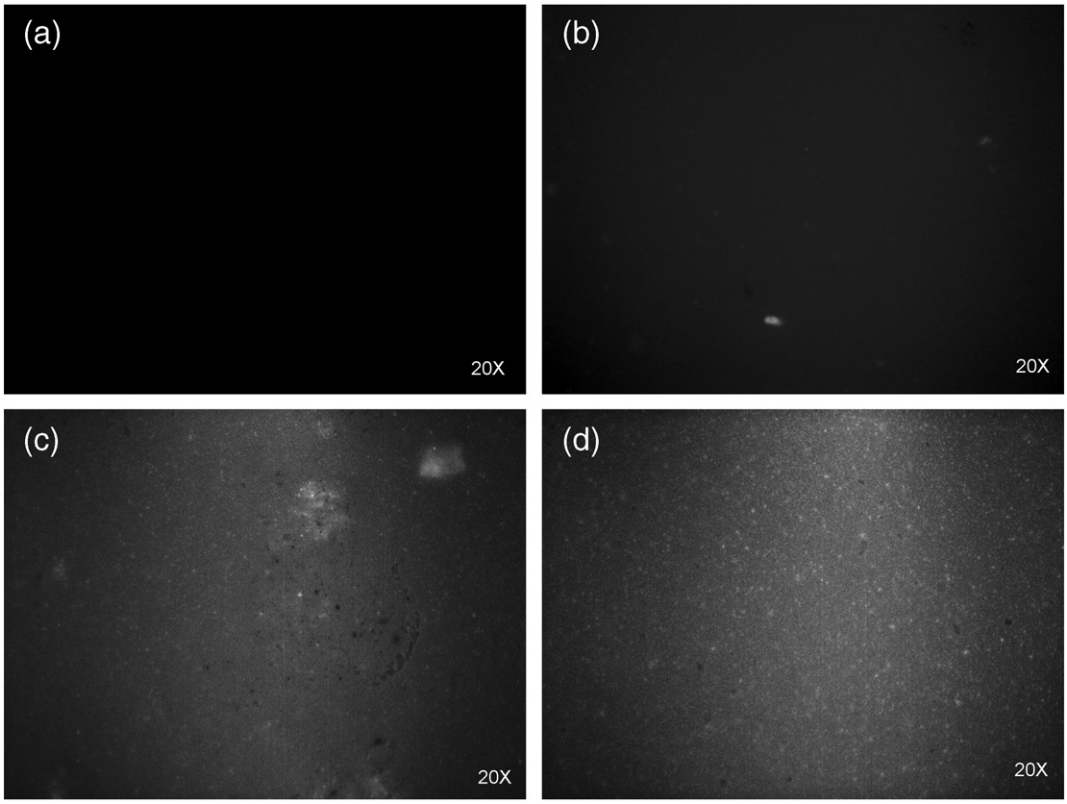

Fig. 1. Fluorescence microscopy of the mixtures before and after adding TMOA at 25 °C and 20×; (a) base asphalt; (b) A/TMOA2; (c) A/TMOA5 and (d) A/TMOA10.

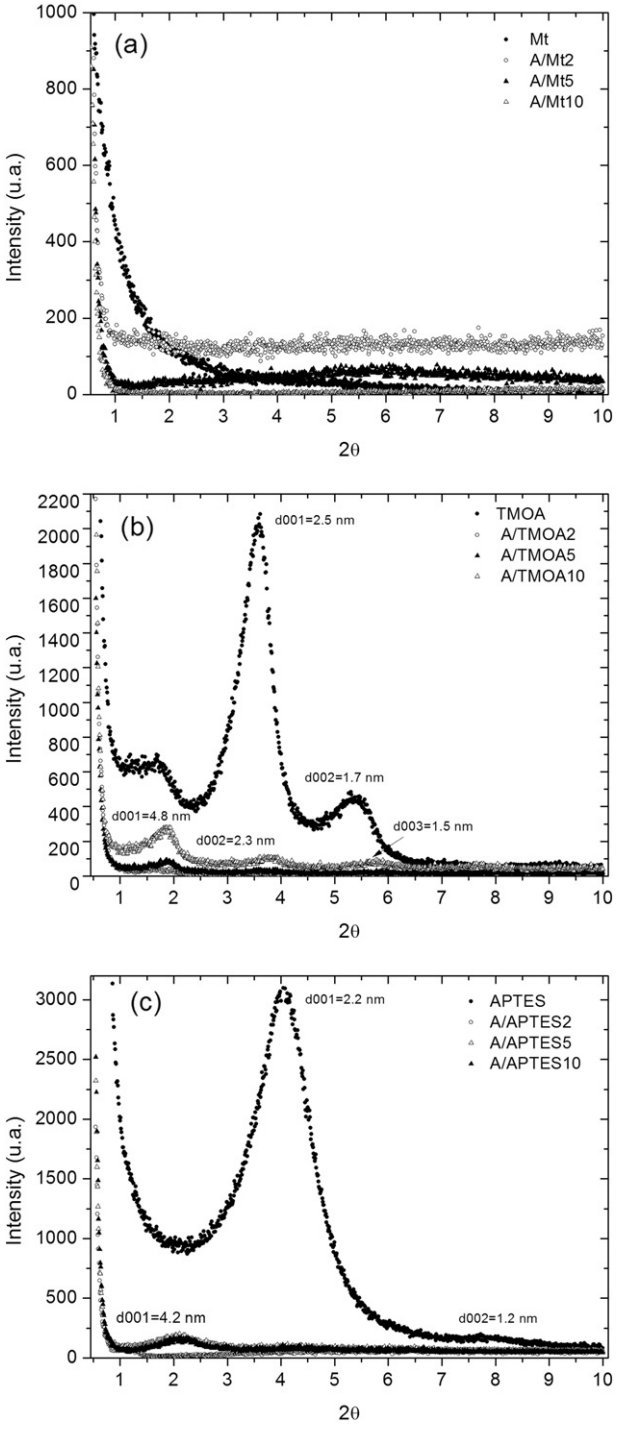

Fig. 2. Basal spacing of the (a) Mt; (b) TMOA and (c) APTES for different concentrations.

Table 2
Diffraction angle and interlayer space at the 001 basal reflection for pure nanoparticles and nanocomposites.

System	2θ (degree)	d (nm)
TMOA	3.58	2.5
A/TMOA2	1.60	5.5
A/TMOA5	1.85	4.8
A/TMOA10	1.85	4.8
APTES	4.08	2.2
A/APTES2	1.1	8.0
A/APTES5	2.1	4.2
A/APTES10	2.2	4.0

reflection (2θ) in the tested interval of 0.5 to 10.0, one cannot suggest that the Mt-modified asphalt forms intercalated or exfoliated structures. Pure TMOA shows a maximum intensity 001 reflections at $2\theta = 3.58°$, which corresponds to a $d = 2.5$ nm, in addition to a small peak at

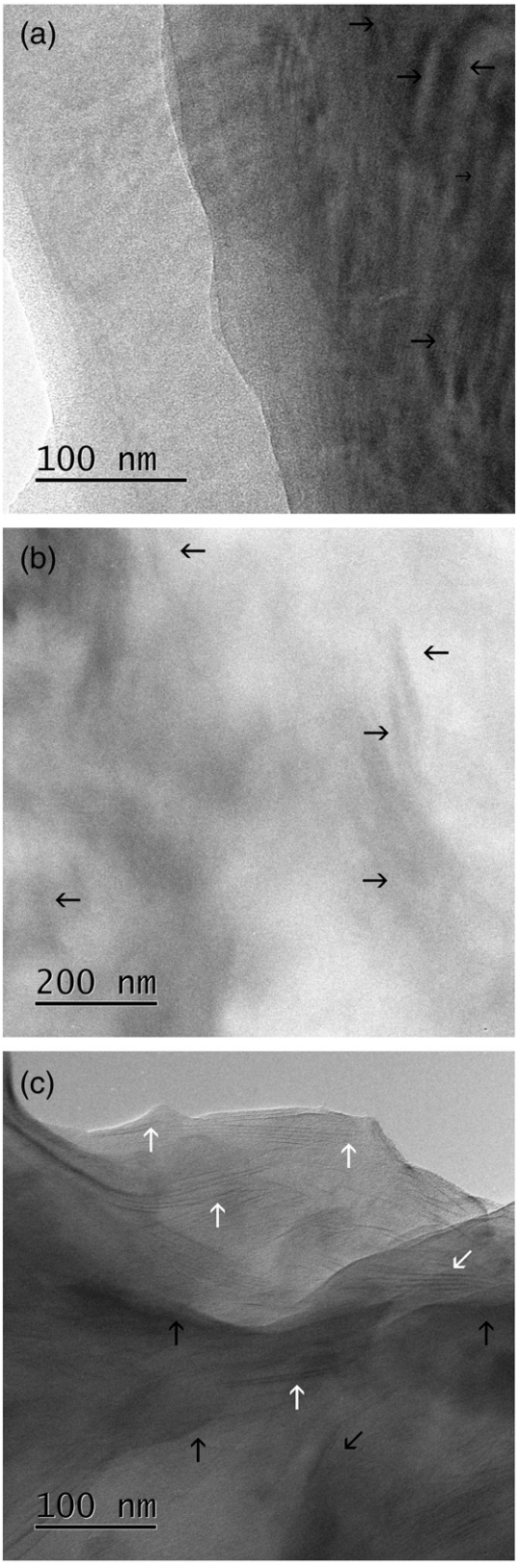

Fig. 3. TEM images of asphalt nanocomposites of (a) Mt; (b) TMOA and (c) APTES at 10 wt.%.

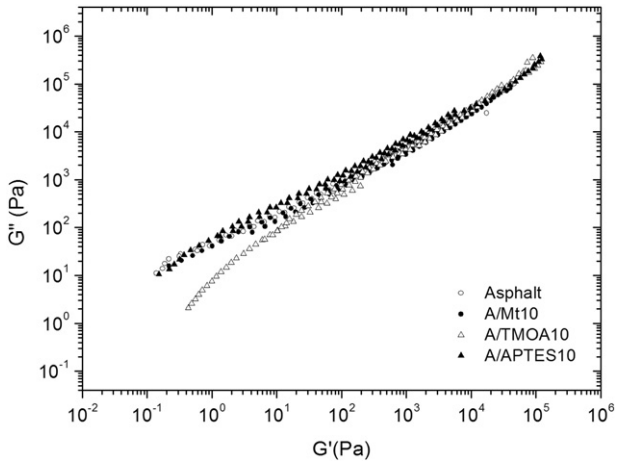

Fig. 4. Plots of log G″ versus log G′, same frequency with 10 wt.% nanoparticles. (a) Mt; (b) TMOA and (c) APTES for various temperatures (100–40 °C).

5.14° (d = 1.7 nm). Lower intensity reflections at high 2θ angles are associated with additional harmonic reflections 002, as they approximately correspond to multiples of the scattering angle of the first order reflection (Okamoto et al., 2000; Yu et al., 2007; Ortega et al., 2015). A/TMOA5 presents two reflections at 2θ = 1.85°, which correspond to d001, and at 3.73° for d002. A/TMOA10 shows three reflections at 2θ = 1.85° for d001, as well as at 3.73° and 5.75°; the higher-order reflections correspond to d002 and d003. These results suggest that TMOA is intercalated in the asphalt matrix. In effect, 001 reflection shifts to a lower angle (Table 2). The large d-value observed can be related to the affinity and/or compatibility between the internal quaternary alkyl ammonium groups attached to the Mt and the asphalt molecules (Ortega et al., 2015). At low nanoparticles content (A/TMOA2) only one reflection is observed at 2θ = 1.6°. X-ray analysis shows an intercalated morphology for all A/TMOA nanocomposites, which gives improvements in the rheological behavior of the material as described above. Pure APTES presents two reflections at 2θ = 4.08° and 7.73°, which correspond to d = 2.2 and 1.15 nm, respectively (Shanmugharaj et al., 2006; Piscitelli et al., 2010; Silva et al., 2011). The A/APTES2 system shows lower basal values of 1.1°, while A/APTES5 and A/APTES10 composites exhibit two reflections at 2θ = 1.9° and 2.0°, respectively, which correspond to d001. In fact, the increase in d-value of 001 from 2.2 nm of APTES to 4.2 nm of A/APTES5 and of A/APTES10 is an evidence of intercalation. The weak reflection at 2θ = 7.7° in pure APTES, which corresponds to d002 (Fig. 2c), disappeared in the diffractograms of A/APTES nanocomposites containing 2, 5, and 10 wt.%. In Table 2, the interlayer space of the A/APTES composites is slightly lower for A/APTES5 and A/APTES10 in comparison to that of A/TMOA5 and A/TMOA10, which explains the different rheological behavior. In effect, viscosity is significantly higher for A/TMOA5 and A/TMOA10 than for A/APTES5 and A/APTES10, as discussed below. The difference in interlayer spacing can be ascribed to the longer organic chains of TMOA, promoting higher interlayer

Table 3
Parameters of Carreau's model for asphalt and nanocomposites.

Sample	η_0 (Pa.s)	η_∞ (Pa.s)	K	m
Asphalt	2.0×10^5	1.1×10^3	4.9×10^1	0.285
A/Mt2	5.2×10^5	1.1×10^3	5.1×10^2	0.110
A/Mt5	6.2×10^5	1.1×10^3	4.6×10^2	0.143
A/Mt10	7.2×10^5	1.1×10^3	4.0×10^2	0.165
A/TMOA2	2.2×10^5	1.1×10^3	2.9×10^2	0.140
A/TMOA5	1.1×10^6	1.1×10^3	3.6×10^2	0.140
A/TMOA10	3.9×10^6	1.1×10^3	8.7×10^3	0.130
A/APTES2	3.4×10^5	1.1×10^3	6.7×10^2	0.098
A/APTES5	5.1×10^5	1.1×10^3	9.0×10^1	0.180
A/APTES10	4.4×10^5	1.1×10^3	2.2×10^2	0.112

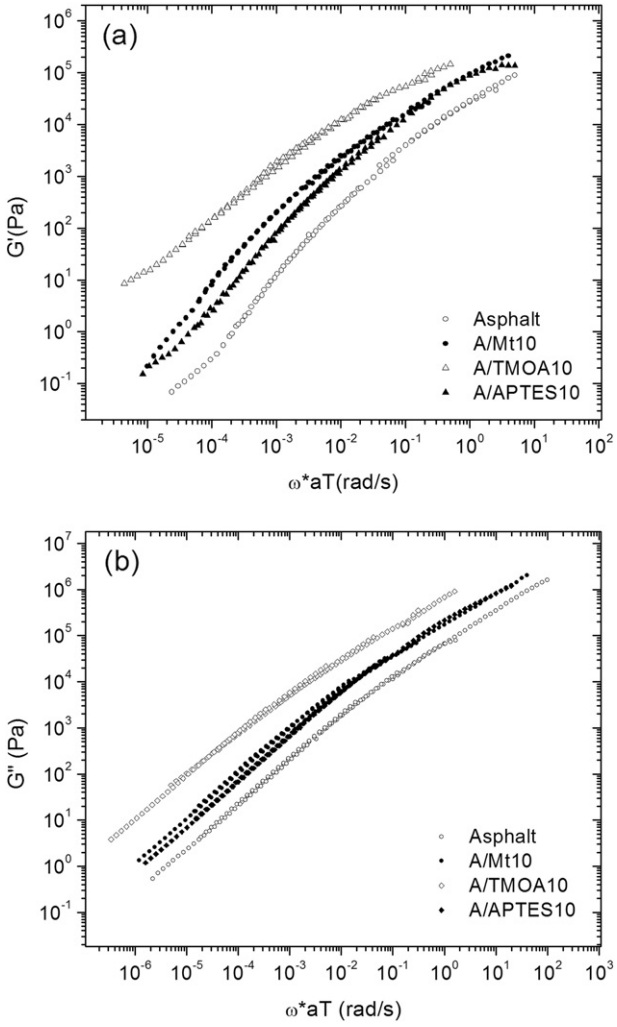

Fig. 5. (a) Storage modulus and (b) loss modulus master curves obtained by time-temperature superposition of asphalt and nanocomposites at 10 wt.% loading. Reference temperature is 25 °C.

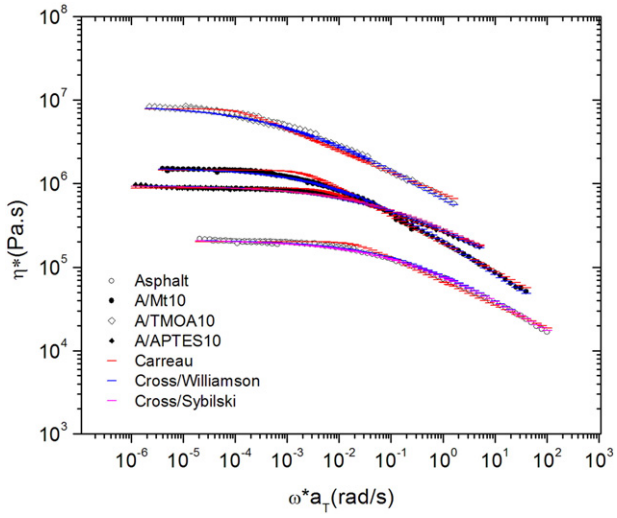

Fig. 6. Complex viscosity (η*) master curves obtained using frequency-temperature superposition at the reference temperature of 25 °C and loading of 10 wt.% nanoparticles. Cross/Williamson, Cross/Sybilski and Carreau models are compared.

Table 4
Parameters of Cross/Williamson's model for asphalt and nanocomposites.

Sample	η_0 (Pa.s)	η_∞ (Pa.s)	K	m
Asphalt	2.1×10^5	1.1×10^3	3.5×10^0	0.42
A/Mt2	1.1×10^6	1.1×10^3	2.0×10^1	0.35
A/Mt5	1.3×10^6	1.1×10^3	4.8×10^1	0.40
A/Mt10	1.5×10^6	1.1×10^3	7.0×10^1	0.45
A/TMOA2	4.7×10^5	1.1×10^3	3.2×10^1	0.40
A/TMOA5	2.4×10^6	1.1×10^3	4.0×10^1	0.45
A/TMOA10	8.6×10^6	1.1×10^3	7.4×10^2	0.38
A/APTES2	7.1×10^5	1.1×10^3	1.2×10^1	0.36
A/APTES5	1.1×10^6	1.1×10^3	1.6×10^1	0.48
A/APTES10	9.4×10^5	1.1×10^3	1.1×10^1	0.38

spacing. According to Shanmugharaj et al. (2006), a reverse trend is observed for aminosilane-Mt systems: the longer the organic chain of the aminosilane molecules, the smaller the d value in the modified Mt. This result is due to the strong tendency of aminosilanes to interact among themselves by both intermolecular hydrogen bonding and hydrophobic interactions due to the presence of one or two —NH groups in their chains, thus revealing the presence of intercalated structures in the base asphalt.

4.4. TEM analysis

TEM images of the nanocomposites at 10 wt.% nanoparticles are shown in Fig. 3. Here, it is important to compare the morphologies and relate them with the rheological and macroscopic properties. In all cases, two different domains are observable: dark zones correspond to nanoparticles, while white zones are asphalt. The structure of the A/Mt10 dispersion is complex (Fig. 3a). Effectively, the overall image shows that the Mt layers are not occupying the full volume, and large regions of pure asphalt matrix are visible. At this scale, considerable inhomogeneity is apparent at high nanoparticle concentration. The nanocomposites exhibit an intercalated morphology and some areas (as indicated by the arrow in Fig. 3a) appear to contain oriented collections of Mt layers (Kormann et al., 1998; Lee et al., 2002; Wang et al., 2008).

In TEM images of A/TMOA 10 wt.% (Fig. 3b) a large number of TMOA intercalated nanoplatelets can be observed, as indicated with black arrows, and irregular dispersions of TMOA layers are present (Wang et al., 2008). Thus, TMOA organo-Mt gives rise to better intercalation as compared to Mt. In turn, the TEM images of A/APTES at 10 wt.% reveal the individual Mt sheets dispersed in asphalt, as shown in Fig. 3c. It is evident that the morphology can be considered a mix of intercalated (as indicated with black arrows) and exfoliated sheets (as indicated with white arrows) in the asphalt matrix (Bharadwaj et al., 2002; Lee and Kim, 2002; Miyagawa et al., 2006). Some regions contain fully-exfoliated structures as they are individually dispersed. However, dispersion of clay in the asphalt matrix becomes slightly worse at 10 wt.%. Thus, silane-grafted located between platelets and edges contribute slightly to platelet dispersion during asphalt processing, while TMOA induces larger separations.

4.5. Rheological analysis

The viscoelastic properties of asphalt and nanocomposites at 10 wt.% of nanoparticles were analyzed in Fig. 4. The loss modulus, $G''(\omega)$, versus storage modulus, $G'(\omega)$, indicates that A/TMOA10 is more elastic than the other nanocomposites. In addition, the $G''(\omega)$ versus $G'(\omega)$ curves of the three nanocomposites with different concentrations and temperatures superpose on a single curve, implying that the nanocomposites do not have a structural heterogeneity (figures were omitted). This indicates that time-temperature superposition for each nanocomposite can be accomplished with a single shift factor, a_T, as described in Eq. (5):

$$a_T = \exp\left[\frac{E_a}{R}\left(\frac{1}{T}-\frac{1}{T_0}\right)\right] \quad (5)$$

where T_0 is the reference temperature, 298 K, and E_a is the activation energy. The activation energy rises with the TMOA and Mt content, while for APTES it remains practically constant (Table 3). E_a is a quantitative mean to evaluate the molecular mobility and increases in the order A/Mt < A/TMOA < A/APTES < Asphalt.

Master curves of dynamic materials functions (G' and G'') for asphalt and nanocomposites at 10 wt.% are shown in Fig. 5. A/TMOA10 wt.% exhibits the highest moduli, implying that this system is more elastic than the other nanocomposites at 10 wt.%. A/TMOA10 sample has the largest interlayer space due to polar interaction between nanoparticles and asphalt. G' and G'' master curves for the nanocomposites A/Mt, A/TMOA and A/APTES increase monotonically with increasing nanoparticles loading (the master curves for these systems are not shown). The presence of nanoparticles does not perturb the general mechanical response of the base asphalt; the dynamic spectra of nanocomposites are similar to that of asphalt, denoting affinity in the rheological behavior of these materials. In comparison, TMOA has a stronger influence on the rheological properties than APTES and Mt. This indicates that the surfactant with ammonium presents stronger interaction with the asphalt matrix.

The viscosity of asphalts strongly depends on its constitutive components and interactions. The presence of solid particles such as Mt, TMOA and APTES in the asphalts matrix contributes to the enhancement of the asphalt viscosity. The steady state flow properties of the nano-Mt modified asphalts are shown in Fig. 6. With the addition of different contents of Mt, TMOA and APTES binders, an increase in η^* of the nanocomposites, particularly at low frequency, is observed. The viscosity of the APTES-modified asphalts increases slightly when the APTES content is increased (one order of magnitude). For TMOA-modified asphalt, intercalated silicate layers can effectively restrict the motion of asphalt chains, which leads to rapid increase of the viscosity. The asphalts modified with high content of TMOA (10 wt.%) show a remarkable increase in η^* by almost two orders of magnitude in comparison to asphalt. The addition of TMOA improves the deformation resistance of asphalt at high temperatures.

Nanocomposites at low frequencies show a Newtonian plateau and for larger shear rates shear-thinning behavior sets in. In nanoparticles-modified asphalts, the shear thinning behavior occurs at a frequency of 10^{-2} to 10^2 rad/s and for asphalt takes place from 10^{-1} to 10^2.

The Carreau's model (Eq. (1)) describes the data obtained from a frequency sweep tests; Fig. 6 and Table 3 disclose the ZSVs of all systems with and without nanoparticles. Fig. 6 reveals that the addition of nanoparticles increases the ZSVs of the binders, especially in TMOA10. The ZSV values calculated from Cross/Williamson and Cross/Sybilski models are consistent; see Tables 4 and 5, respectively. However, the ZSV values

Table 5
Parameters of Cross/Sybilski's model for asphalt and nanocomposites.

Sample	η_0 (Pa.s)	K	m
Asphalt	2.1×10^5	4.0×10^0	0.40
A/Mt2	1.1×10^6	1.6×10^1	0.38
A/Mt5	1.4×10^6	5.3×10^1	0.40
A/Mt10	1.6×10^6	9.0×10^1	0.42
A/TMOA2	4.8×10^5	2.8×10^1	0.40
A/TMOA5	2.5×10^6	4.0×10^1	0.40
A/TMOA10	8.7×10^6	8.6×10^2	0.38
A/APTES2	7.1×10^5	1.2×10^1	0.35
A/APTES5	1.1×10^6	1.5×10^1	0.47
A/APTES10	9.3×10^5	9.0×10^0	0.38

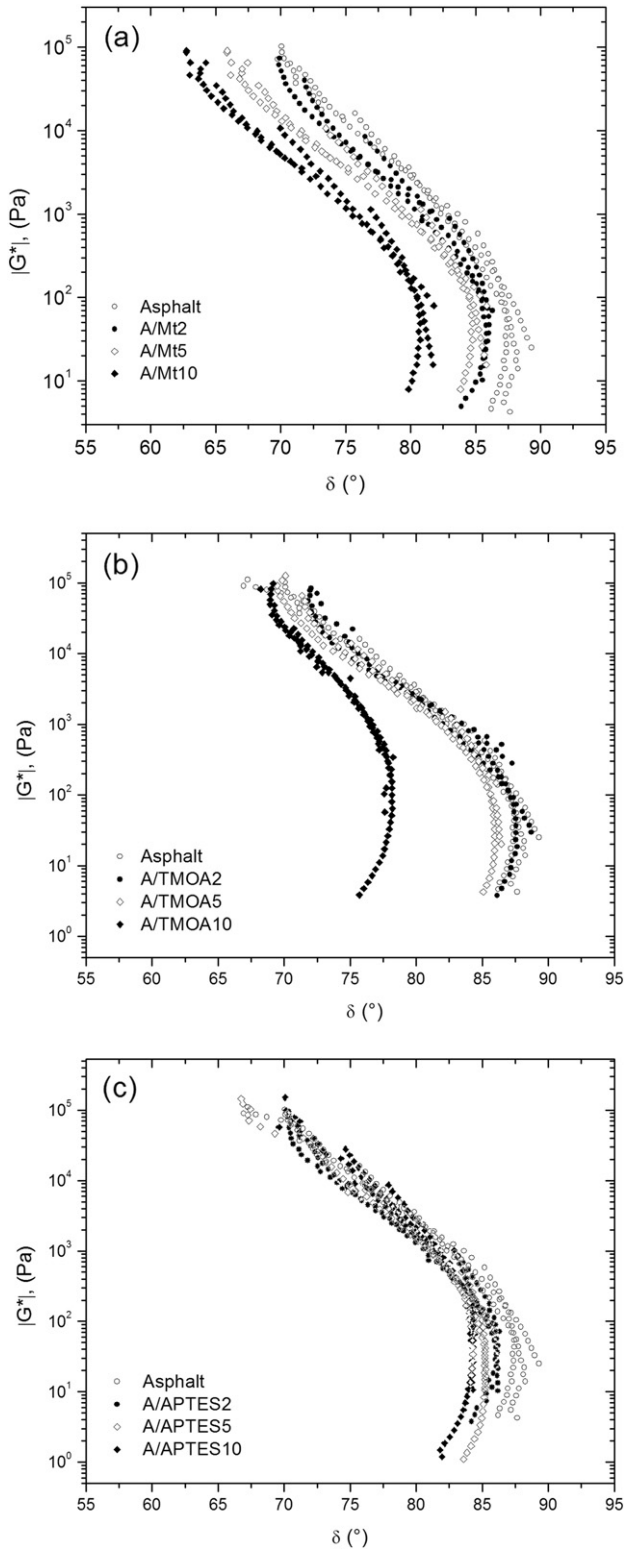

Fig. 7. Black diagrams of asphalt and blends reinforced with nanoparticles for various concentrations; (a) Mt; (b) TMOA; and (c) APTES.

calculated for TMOA are significantly higher than the ZSV values calculated for Mt, APTES and asphalt.

Black diagrams are plotted for each system in Fig. 7. Black diagrams of neat asphalt and nanocomposites are very similar; the overall rheological behavior is not affected by the presence of nanoparticles. For A/TMOA and A/Mt blends, an increase in the amount of reinforcement improves the stiffness and elasticity (phase angles decreases and moduli increases). The use of APTES does not yield the same rheological effects, since Black diagrams are similar to those of asphalt (Fig. 7a–c). In this case, a slight departure from the thermo-rheological simplicity of the material is observed, associated to the presence of strong nanoparticle structures within the dispersing medium (Santagata et al., 2015). These blends present a slight improvement in the elasticity and stiffness with respect to asphalt.

Table 6
Maximum pavement temperature obtained by SHRP criterion for all samples.

Samples	Temperature when $G^*/\sin\delta = 1$ kPa (°C)
Asphalt	70
A/Mt2	74
A/Mt5	78
A/Mt10	84
A/TMOA2	72
A/TMOA5	87
A/TMOA10	92
A/APTES2	73
A/APTES5	75
A/APTES10	75

SHRP criterion indicates the maximum temperature for a good viscoelastic performance of the original binder once in the pavement (defined as the point when $|G^*|/\sin\delta$ attains 1 kPa at 10 rad/s). To define the maximum pavement temperature, the analysis related to aging of the RTFOT asphalt binder is needed. Values of these points are shown in Table 6 for asphalt and blends. The addition of nano-additives always leads to improvements in the resistance to permanent deformation of asphalt. As the nanoparticles content increases, the temperature of the SHRP parameter increases. The best temperature performances are found by employing TMOA at high concentrations, while APTES shows lower ability to affect rheological properties of asphalt, like Mt2 and Mt5. It is noteworthy that high dosages of TMOA and Mt at 10 wt.% lead to high values of the SHRP rutting resistance factor.

5. Conclusions

The addition of nanoclays to asphalt decreases penetration and increases both the softening point and viscosity. XRD and TEM analyses reveal the degree of intercalation and dispersion of montmorillonite in asphalt. XRD data confirm that the organo-Mt-modified asphalt may form an intercalated structure, while this structure cannot be corroborated for A/Mt composites, since Mt does not show XRD dispersion peaks in the interval selected in this work. The changes in the rheological properties of the modified asphalt depend on the type and concentration of nanocomposite, and its distribution in the asphalt. The modified asphalts exhibited higher complex modulus, lower phase angle and higher rutting resistance. Compared with Mt and APTES, TMOA has larger effects in improving physical properties and rutting resistance of asphalt, due to the formation of intercalated structures in the TMOA-modified asphalt and the better surface compatibility of TMOA nanoparticles with the asphalt. Both the Cross and Carreau models can describe the viscosity of asphalt and asphalt binder. Similar ZSV values are obtained using various constitutive models.

Acknowledgements

The authors want to thank CONACyT-México for providing financial support under Project INFR-2011-1-163250. Also special thanks to Lab XRD (T-128) UAM-I for SAXS measurements. Acknowledgements are given to Ing. Patricia Castillo for the obtainment of TEM images.

References

Bharadwaj, R.K., Mehrabi, A.R., Hamilton, C., Trujillo, C., Murga, M., Fan, R., Chavira, A., Thompson, A.K., 2002. Structure-property relationships in cross-linked polyester-clay nanocomposites. 43, 3699–3705.

Biro, S., Gandhi, T., Amirkhanian, S., 2009. Determination of zero shear viscosity of warm asphalt binders. Constr. Build. Mater. 23, 2080–2086.

Chen, Z., Zhang, H., Zhu, C., Zhao, B., 2015. Rheological examination of aging in bitumen with inorganic nanoparticles and organic expanded vermiculite. Constr. Build. Mater. 101, 884–891.

Drozdov, A.D., Jensen, E.A., Christiansen, J.C., 2008. Thermo-viscoelastic response of nano-composite melts. Int. J. Eng. Sci. 46, 87–104.

El-Shafie, M., Ibrahim, I.M., Abd El Rahman, A.M.M., 2012. The addition effects of macro and nano clay on the performance of asphalt binder. Egypt. J. Pet. 21, 149–154.

Fang, C., Yu, R., Liu, S., Li, Y., 2013. Nanomaterials applied in asphalt modification: a review. J. Mater. Sci. Technol. 29 (7), 589–594.

Golestani, B., Nejad, F.M., Galooyak, S.S., 2012. Performance evaluation of linear and non-linear nanocomposite modified asphalts. Constr. Build. Mater. 35, 197–203.

Golestani, B., Nam, B.H., Nejad, F.M., Fallah, S., 2015. Nanoclay application to asphalt concrete: characterization of polymer and linear nanocomposite-modified asphalt binder and mixture. Constr. Build. Mater. 91, 32–38.

Jahromi, S.G., Khodaii, A., 2009. Effects of nanoclay on rheological properties of bitumen binder. Constr. Build. Mater. 23, 2894–2904.

Jahromi, S.G., Andalibizade, B., Vossough, S., 2010. Engineering properties of nanoclay modified asphalt concrete mixtures. Arab. J. Sci. Eng. 35 (1), 89–103.

Kakehi, K., Maeya, Y.K., Oda, Y., Hayase, S., 1997. Use of a binary mixture of quaternary ammonium salts in fluorometric determination of glycosaminoglycans. Anal. Biochem. 252 (1), 56–61.

Kormann, X., Berglund, L.A., Sterte, J., 1998. Nanocomposites based on montmorillonite and unsaturated polyester. Polym. Eng. Sci. 38 (8), 1351–1358.

Lee, S.Y., Kim, S.J., 2002. Delamination behavior of silicate layers by adsorption of cationic surfactants. J. Colloid Interface Sci. 248, 231–238.

Lee, S.R., Park, H.M., Lim, H., Kang, T., Li, X., Cho, W.J., Ha, C.S., 2002. Microstructure. Tensile properties, and biodegradability of aliphatic polyester/clay nanocomposites. Polymer 43, 2495–2500.

Liu, G., Wu, S., van de Ven, M., Yu, J., Molenaar, A., 2010. Influence of sodium and organo-montmorillonites on the properties of bitumen. Appl. Clay Sci. 49, 69–73.

Liu, G., Wu, S., van de Ven, M., Yu, J., Molenaar, A., 2013. Structure and artificial ageing behavior of organomontmorillonite bitumen nanocomposites. Appl. Clay Sci. 72, 49–54.

Merusi, F., Giuliani, F., Polacco, G., 2012. Linear viscoelastic behavior of asphalt binders modified with polymer/clay nanocomposites. Procedia. Soc. Behav. Sci. 53, 335–345.

Min, Y., Fang, Y., Huang, X., Zhu, Y., Li, W., Yuan, J., Tan, L., Wang, S., Wu, Z., 2015. Surface modification of basalt with silane coupling agent on asphalt mixture moisture damage. Appl. Surf. Sci. 346, 497–502.

Miyagawa, H., Drzal, L.T., Carsello, J.A., 2006. Intercalation and exfoliation of clay nanoplatelets in epoxy-based nanocomposites: TEM and XRD observations. Polym. Eng. Sci. 46, 452–463.

Morea, F., Agnusdei, J.O., Zerbino, R., 2010. Comparison of methods for measuring zero shear viscosity in asphalts. Mater. Struct. 43, 499–507.

Okamoto, M., Morita, S., Taguchia, H., Kima, Y.H., Kotakaa, T., Tateyama, H., 2000. Synthesis and structure of smectic clay/poly(methyl methacrylate) and clay/polystyrene nanocomposites via in situ intercalative polymerization. Polymer 41, 3887–3890.

Ortega, F.J., Navarro, F.J., García-Morales, M., McNally, T., 2015. Thermo-mechanical behavior and structure of novel bitumen/nanoclay/MDI composites. Compos. Part B 76, 192–200.

Piscitelli, F., Posocco, P., Toth, R., Fermeglia, M., Pricl, S., Mensitieri, G., Lavorgna, M., 2010. Sodium montmorillonite silylation: Unexpected effect of the aminosilane chain length. J. Colloid Inter. Sci. 351, 108–115.

Polacco, G., Kriz, P., Filippi, S., Stastna, J., Biondi, D., Zanzotto, L., 2008. Rheological properties of asphalt/SBS/clay blends. Eur. Polym. J. 44 (11), 3512–3521.

Santagata, E., Baglieri, O., Tsantilis, L., Chiappinelli, G., Aimonetto, I.B., 2015. Effect of sonication on high temperature properties of bituminous binders reinforced with nano-additives. Constr. Build. Mater. 75, 395–403.

Shanmugharaj, A.M., Rhee, K.Y., Ryu, S.H., 2006. Influence of dispersing medium on grafting of aminopropyltriethoxysilane in swelling clay materials. J. Colloid Interface Sci. 298, 854–859.

Silva, A.A., Dahmouche, K., Soares, B.G., 2011. Nanostructure and dynamic mechanical properties of silane-functionalized montmorillonite/epoxy nanocomposites. Appl. Clay Sci. 54, 151–158.

Sureshkumar, M.S., Filippi, S., Polacco, G., Kazatchkov, I., Stastna, J., Zanzotto, L., 2010. Internal structure and linear viscoelastic properties of EVA/asphalt nanocomposites. Eur. Polym. J. 46, 621–633.

Wang, W.S., Chen, H.S., Wu, Y.W., Tsai, T.Y., Chen-Yang, Y.W., 2008. Properties of novel epoxy/clay nanocomposites prepared with a reactive phosphorus-containing organoclay. Polymer 49, 4826–4836.

Yang, J., Tighe, S., 2013. A review of advances of nanotechnology in asphalt mixtures. Procedia. Soc. Behav. Sci. 96, 1269–1276.

Yao, H., You, Z., Li, L., Shi, X., Goh, S.W., Mills-Beale, J., Wingard, D., 2012. Performance of asphalt binder blended with non-modified and polymer-modified nanoclay. Constr. Build. Mater. 35, 159–170.

Yao, H., You, Z., Li, L., Lee, C.H., Wingard, D., Yap, Y.K., Shi, X., Goh, S.W., 2013. Rheological properties and chemical bonding of asphalt modified with nanosilica. J. Mater. Civ. Eng. 25 (11), 1619–1630.

You, Z., Mills-Beale, J., Foley, J.M., Roy, S., Odegard, G.M., Dai, Q., Wei Goh, S., 2011. Nanoclay-modified asphalt materials: preparation and characterization. Constr. Build. Mater. 25, 1072–1078.

Yu, J.Y., Zeng, X., Wu, S.P., 2007. Preparation and properties of montmorillonite modified asphalts. Mater. Sci. Eng. A 447, 233–238.

Yu, J.Y., Feng, P.C., Zhang, H.L., Wu, S.P., 2009. Effect of organo-montmorillonite on aging properties of asphalt. Constr. Build. Mater. 23, 2636–2640.

Zare-Shahabadi, A., Shokuhfar, A., Ebrahimi-Nejad, S., 2010. Preparation and rheological characterization of asphalt binders reinforced with layered silicate nanoparticles. Constr. Build. Mater. 24, 1239–1244.

Zhang, H., Yu, J., Wang, H., Xue, L., 2011. Investigation of microstructures and ultraviolet aging properties of organo-montmorillonite/SBS modified bitumen. Mater. Chem. Phys. 129, 769–776.